Glass Transition Line in C_{60}: A Mode-Coupling/Molecular-Dynamics Study

D. Costa,*,† R. Ruberto,†,‡ F. Sciortino,§ M. C. Abramo,† and C. Caccamo†

Dipartimento di Fisica, Università di Messina and CNISM Ctr Papardo, 98166 Messina, Italy, CNR-INFM DEMOCRITOS National Simulation Center and Dipartimento di Fisica Teorica, Università di Trieste Strada Costiera 11, 34014 Trieste, Italy, and Dipartimento di Fisica, Università di Roma "La Sapienza", Piazzale Aldo Moro 2, 00185 Roma, Italy

Received: March 19, 2007; In Final Form: June 5, 2007

We report a study of the mode-coupling theory (MCT) glass transition line for the Girifalco model of C_{60} fullerene. The equilibrium static structure factor of the model, the only required input for the MCT calculations, is provided by molecular dynamics simulations. The glass transition line develops inside the metastable liquid−solid coexistence region and extends down in temperature, terminating on the liquid side of the metastable portion of the liquid−vapor binodal. The vitrification locus does not show re-entrant behavior. A comparison with previous computer simulation estimates of the location of the glass line suggests that the theory accurately reproduces the shape of the arrest line in the density-temperature plane. The theoretical HNC and MHNC structure factors (and consequently the corresponding MCT glass line) compare well with the numerical counterpart. Our results confirm the conclusion drawn in previous works about the existence of a glassy phase for the fullerene model at issue.

1. Introduction

The onset of a glassy phase characterized by positional disorder in the Girifalco central potential model of C_{60}[1] has been recently documented by some of us via molecular dynamics (MD) studies.[2,3] Interest in the vitrification process in fullerenes stems not only from the intrinsic relevance of this class of materials but also from the nature of their interparticle interaction. The Girifalco potential appears in fact to be "marginally" short-range, giving rise to peculiar effects when we consider the interplay between the decay of the interactions and both the characteristics of the phase portrait and the glass forming ability of this model. In particular, following an initial debate on the existence of a stable liquid phase for this model,[4,5] it has been shown that the liquid pocket in the C_{60} phase diagram is confined to a tiny temperature interval (see, e.g., refs 6 and 7 and references therein). In this sense, the system displays a characteristic "borderline" behavior, intermediate between what one expects for the phase equilibria of a simple fluid (with a fully developed liquid phase) and a condition where the liquid−vapor equilibrium is only metastable with respect to the vapor-solid phase separation, the binodal curve falling below the sublimation line. The latter behavior is usually observed when the range of attractive forces is short enough compared with the size of the repulsive core, a condition typically faced when one considers effective models for macrosized molecular systems, like protein solutions[8−10] or colloidal suspensions.[11]

On the other hand, extensive studies of the glass transition in simple systems like square wells, adhesive hard spheres, and hard-core Yukawa fluids[12−14] (see ref 15 for a recent review), based on the application of the mode-coupling theory (MCT[16]) have identified two distinct mechanisms of formation of glasses according to the balance of the repulsive and attractive interactions. In particular, systems with sufficiently short-range attraction exhibit, together with a normal repulsion-driven glass which behaves qualitatively like a hard-sphere glass, an "attractive" glass of a different nature, favored both by the energy and the local entropy.[17,18] This circumstance naturally candidates the C_{60} model, wherein, as observed, the subtleties related to the shape of the interaction potential play a crucial role, for a study of the glass transition and of its typicality.

Besides our simulations investigations,[2,3] the study of the glass transition line in the Girifalco model has been recently addressed by Greenall and Voigtmann.[19] In ref 19, these authors carry out ideal MCT calculations, using as input data for the theory the static structure factors $S(k)$ obtained from the hypernetted chain (HNC) and Percus−Yevick (PY) liquid state theories.[20] They show that vitrification in the C_{60} model occurs, in agreement with MD results, although at densities lower than those predicted by the computer simulations; such an underestimate is not unexpected given the inherent inaccuracies of MCT.[14] Moreover, the features of the MCT non-ergodicity parameter and the overall behavior of the glass transition line indicate the crossover to an attractive-glass behavior at relatively low temperatures, thereby expanding the scenario emerging from previous simulations. MD simulations have shown in fact evidence of a repulsive glass only, over the whole temperature range investigated.[2,3] The possibility that an attractive glass can exist for the Girifalco model appears somewhat unexpected on the basis of the broad analysis carried out in ref 14, in which a Yukawa model with parameters compatible with the decay rate of the Girifalco potential displays a repulsive glass only. A similar conclusion is drawn in ref 19 itself: if one uses a square-well potential mimicking the attraction range of the Girifalco model, the resulting interaction is not short-range enough to determine the appearance of an attraction-driven glass.

The possibility that the attractive interaction in the Girifalco model is sufficiently short-range to display several peculiar features of an attractive glass poses intriguing questions about

* Corresponding author. E-mail: dino.costa@unime.it.
† Università di Messina and CNISM Ctr Papardo.
‡ Università di Trieste Strada Costiera.
§ Università di Roma "La Sapienza".

10.1021/jp072186v CCC: $37.00
Published on Web 08/17/2007

the whole mechanism which underlies the existence of such an arrested state of matter, with implications for a variety of similar potentials currently used in colloid and protein studies. On the other hand, the arguments put forward in ref 19 hinge on two approximate liquid state approaches, like the HNC and the PY theories, and on a previous analysis carried out by the same authors,[21] about the (weak) sensitivity of MCT predictions to the $S(k)$ behavior in the low-k region, below the first diffraction peak. This scenario motivates in our opinion an investigation of MCT predictions implemented through the use of accurate structure factors. We have performed to this aim extensive MD calculations in the temperature and density regimes inside the vapor−solid and liquid−solid regions and extracted the structure factor directly from the simulation data, down to the lowest k vector compatible with the simulation box size. In order to assess the theoretical predictions, we have also calculated the static structure factor in some selected thermodynamic state points, in the framework of the modified HNC (MHNC[22]) approach, a theory which yields accurate results for the C_{60} model.[23]

The paper is organized as follows: section 2 is devoted to an introduction of the model, of the simulations strategy, and of the basic equations employed in the MCT. In section 3, results are reported and discussed, and section 4 contains a few concluding remarks.

2. Model, Simulation Procedure and MCT Approach

The Girifalco interaction potential $v(r)$ among two C_{60} molecules reads[1]

$$v(r) = -\alpha_1\left[\frac{1}{s(s-1)^3} + \frac{1}{s(s+1)^3} - \frac{2}{s^4}\right] + \alpha_2\left[\frac{1}{s(s-1)^9} + \frac{1}{s(s+1)^9} - \frac{2}{s^{10}}\right] \quad (1)$$

where $s = r/d$, $\alpha_1 = N^2A/12d^6$, and $\alpha_2 = N^2B/90d^{12}$; $N = 60$ and $d = 0.71$ nm are the number of carbon atoms and the diameter, respectively, of the fullerene particles; $A = 32 \times 10^{-60}$ erg cm^6 and $B = 55.77 \times 10^{-105}$ erg cm^{12} are constants entering the 12−6 potential $\phi(r) = -A/r^6 + B/r^{12}$ through which two carbon sites on different spherical molecules are assumed to interact. The distance where the potential in eq 1 crosses zero, the position of the potential well minimum, and its depth are $\sigma = 0.959$ nm, $r_{min} = 1.005$ nm, and $\epsilon = 0.444 \times 10^{-12}$ erg, respectively.

MD simulations are carried out on a system composed of 1000 particles enclosed in a cubic box with periodic boundary conditions. The Andersen algorithm[24] is used to enforce constant-pressure P and constant-enthalpy H conditions to the sample. We have analyzed the system along the cooling paths characterized by the pressure $P = 3$, 5, 40, 150, and 250 MPA, according to the strategy already documented in refs 2 and 3. As visible in Figure 1, five to seven thermodynamic states for each pressure are selected around the glass transition points (which have been estimated through several structural and dynamic indicators in ref 3), and long trajectories are generated to estimate the equilibrium static structure factor $S(k)$ to be fed into the mode-coupling theory calculations. Several state points along the isotherms $T = 1200$ and 3500 K are also analyzed, in order to characterize the behavior of the vitrification curve in the limits of relatively low and high temperatures (see Figure 1).

Runs of 12 000 time steps (with $\Delta t = 5$ fs) are generally long enough to ensure a stable estimate of structure factors. Two method for the calculation of $S(k)$ (namely through a direct estimate of fluctuations of the density ρ and by Fourier inversion of the radial distribution function $g(r)$) are used and compared in this study. Results are generally equivalent: the calculations coming from $g(r)$ are on the whole less noisy than those obtained through the direct method, whereas the latter are more accurate in the small-k region. If necessary, a smoothing procedure has been applied to the $S(k)$ data prior to mode-coupling calculations.

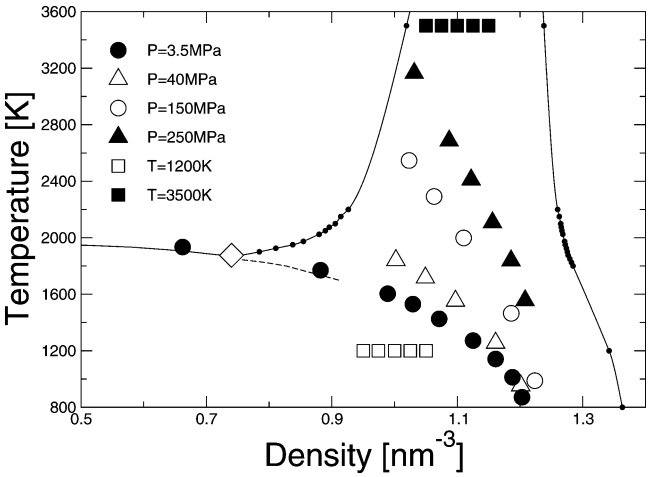

Figure 1. Cooling paths at $P = 3.5$, 40, 150, and 250 MPa and constant temperature runs at $T = 1200$ and 3500 K. Full lines correspond to the liquid branch of the binodal and the liquid−solid coexistence lines.[6] The triple point (diamond) and the metastable portion of the binodal line (dashed curve) are also shown. Dots collectively show all past[6] and newly added (see text) estimates of coexistence points.

MCT derives equations for the normalized time-dependent density correlators of the Fourier components of the particle density fluctuations $\delta\rho_k(t)$[16]

$$\Phi_k(t) \equiv \frac{\langle \delta\rho_k(t)\delta\rho_{-k}(0)\rangle}{\langle |\delta\rho_k|^2\rangle} \quad (2)$$

starting only from the number density ρ and the structure factor $S_k = \langle|\delta\rho_k|^2\rangle/N$ (or equivalently the direct correlation function $\rho c_k = 1 - S_k^{-1}$. The glass transition predicted by MCT is obtained solving the $t \rightarrow \infty$ limit of the equations for the normalized correlators $\Phi_k(t)$, the so-called non-ergodicity factor f_k

$$f_k = \lim_{t\rightarrow\infty} \Phi_k(t) \quad (3)$$

The equations have the form

$$\lim_{t\rightarrow\infty} m_k(t) = \frac{f_k}{1 - f_k} \quad (4)$$

where the memory kernel is given by

$$m_k(t) = \frac{\rho}{V}\sum_{k'\neq k} S_k S_{|k-k'|} S_{k'} \left|\frac{\mathbf{k}\cdot\mathbf{k}'}{k^2} c_{k'} + \frac{\mathbf{k}\cdot(\mathbf{k}-\mathbf{k}')}{k^2} c_{k-k'}\right|^2 \Phi_{|k-k'|}(t)\Phi_{k'}(t) \quad (5)$$

For specific values of the input parameters, the solution to these equations admits not only the usual trivial solution $f_k = 0$, but also solutions with $f_k \neq 0$. The value of f_k at the transition point

is denoted f_k^c. We have solved eqs 4 and 5 on a grid of 300 wavevectors up to $k = 32$ nm^{-1} using a standard iterative procedure.

3. Results

An overview of all state points encompassed in this work is reported in Figure 1, in the context of the phase diagram of the C_{60} model calculated in ref 6. Newly generated fluid−solid coexistence points in the high-temperature regime ($T = 3500$ K) and in the low temperature solid phase ($T \leq 1200$ K) are displayed as well, in order to elucidate the whole appearance of the coexistence region where all calculations have been done. The coexistence points at high temperature are in particular calculated according to the procedure employed in ref 25: the free energy of the fluid phase is calculated through thermodynamic integration of the MD pressure at several state points along the isotherm $T = 3500$ K, whereas for the solid phase, we have used a first-order perturbation theory starting from a crystal of hard spheres, whose diameter is chosen according to the Weeks−Chandler−Andersen (WCA) procedure.[26] We have obtained in this way for the coexisting densities: $\rho_{\text{fluid}}(T = 3500) = 1.02$ nm^{-3} and $\rho_{\text{solid}}(T = 3500) = 1.24$ nm^{-3}. As for the isotherms $T = 1200$ and 800 K, we have assumed that the coexisting solid density must be that where the (perturbation theory) pressure reduces to zero: a simple approximation justified by the fact that in this regime the coexisting vapor density is extremely low and thus it plausibly corresponds to almost zero pressure. We have obtained $\rho_{\text{solid}}(T = 1200) = 1.34$ nm^{-3} and $\rho_{\text{solid}}(T = 800) = 1.36$ nm^{-3}.

As visible from Figure 1, thermodynamic states at pressures increasingly higher than $P = 3.5$ MPa are allocated between the freezing and the melting lines of the model. State points along the isobaric path $P = 3.5$ MPa are almost superimposed on the liquid branch of the metastable portion of the liquid−vapor phase separation, whereas all thermodynamic states along the isotherm $T = 1200$ K are definitely inside the vapor−solid coexistence region. This point can be further illustrated by the evaluation of the structure factors at $T = 1200$ K and $P = 3.5$ MPa, reported in Figure 2. It appears that the structure factor at $T = 1200$ K is barely sensitive to density variations in the range 0.95−1.05 nm^{-3} but for the steep rise of the $k \rightarrow 0$ limit when the density is decreased, clearly indicating a more and more pronounced tendency of the sample to phase separate as it goes deeper and deeper inside the (metastable) binodal. On the other hand, the structure factor at $P = 3.5$ MPa stays around zero in the $k \rightarrow 0$ limit and becomes more structured during the cooling sequence documenting in this way the approach to the solid configuration.

In parallel, the spatial configurations obtained at $T = 1200$ K, analyzed in terms of nearest-neighbors distributions of particles and by means of a direct visual inspection, reveals at $\rho = 0.95$ nm^{-3} the existence of a rarefact region in the sample surrounded by a uniformly denser environment (see the snapshot in Figure 3). Such strong dishomogeneities tend to persist almost up to $\rho = 1.025$ nm^{-3} and disappear at higher densities: at $\rho = 1.05$ nm^{-3}, we have detected no evidence of (incipient) phase separation, and the system displays a uniform distribution of particles inside the simulation box.

At variance with the latter regime, all other points investigated in this work represent truly equilibrated thermodynamic states. In order to be sure that all samples are properly equilibrated and that each particle diffuses on average more than its diameter over the whole simulation time, we have recorded the mean square displacement (MSD) over particularly long simulation runs for some selected state points where MCT predicts the glass transition. Results are reported in Figure 4: as visible, observation windows of the order of ∼0.1 ns allow the particles to diffuse for a distance varying between ∼1.4 and ∼1.7 molecular diameters, the latter being roughly identified with the "colli-

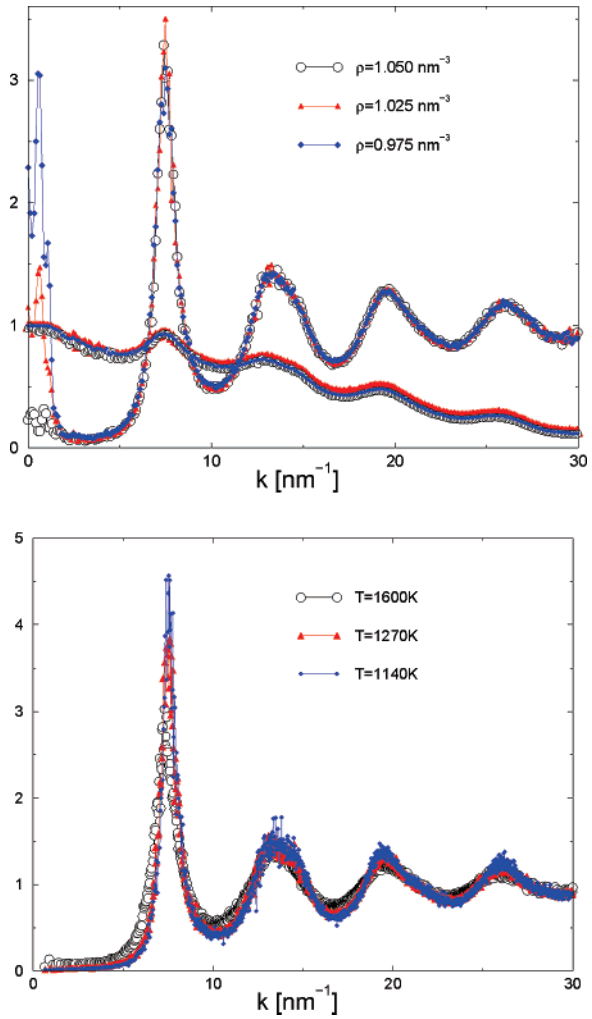

Figure 2. MD static structure factors along the $T = 1200$ K (top) and $P = 3.5$ MPa (bottom) paths. In the top panel, the corresponding nonergodicity factors are also displayed.

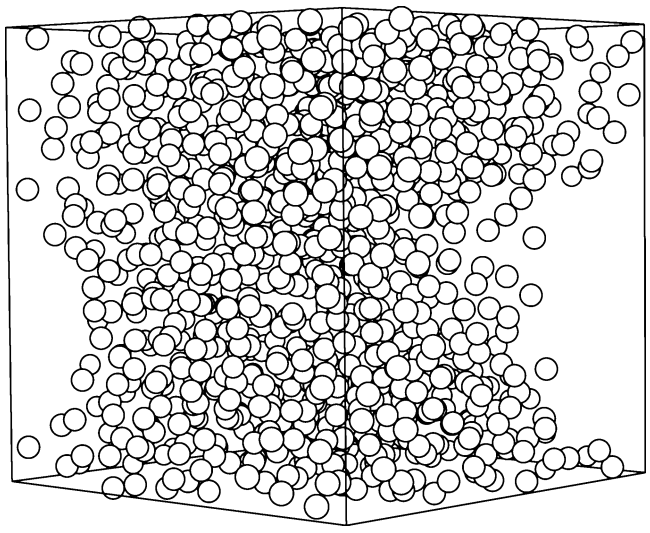

Figure 3. Snapshot of the final configuration of the system at $T = 1200$ K and $\rho = 0.95$ nm^{-3}; a void region clearly displays in the sample.

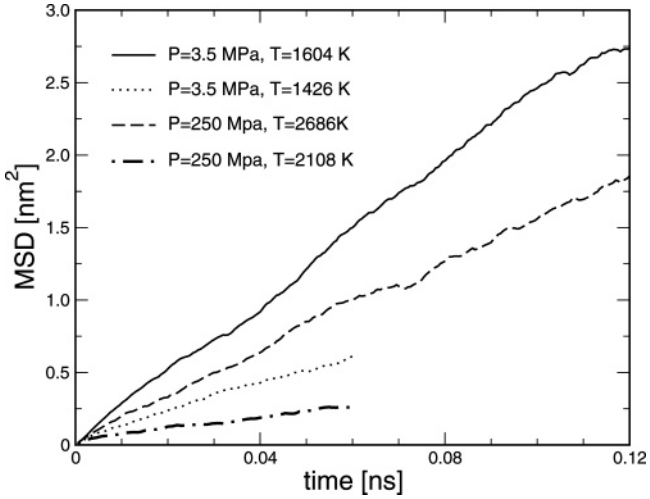

Figure 4. Mean square displacements across the MCT vitrification thresholds at $P = 3.5$ and 250 MPa. Longer runs correspond to the states immediately before the transition point.

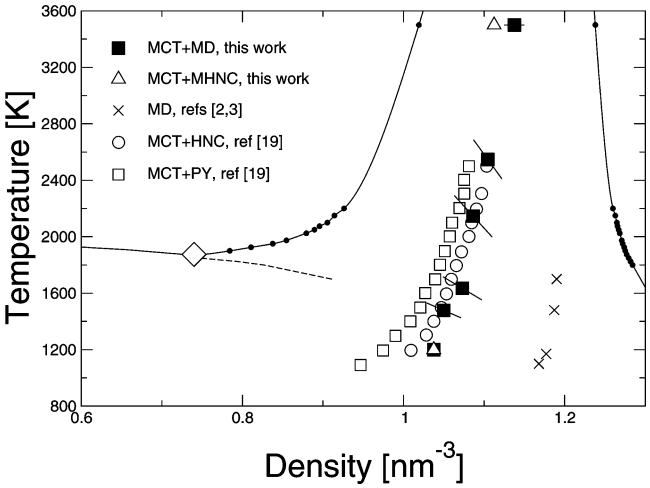

Figure 5. Glass transition points obtained in this work through MCT calculations based on MD (full squares) and MHNC (triangles) structure factors. Error bars on MCT/MD data are given by the separation between the last ergodic and the first nonergodic state points along the isobaric or the isothermal paths followed during the MD sequences (see text and Figure 1 for more details). Crosses are the glass transition estimates through direct MD calculations.[2,3] MCT predictions of ref 19 with HNC (circles) and PY (open squares) structure factors are also shown. All data are reported in the context of the phase diagram of the C_{60} model, represented by the full lines with dots, the dashed line, and the diamond (see caption of Figure 1 for symbols).

sional" distance σ of the C_{60} potential (see section 2). The diffusion coefficient varies between $\sim 2.6 \times 10^{-5}$ and 3.8×10^{-5} cm^2/s before the MCT transition and drops to $\sim 1.6 \times 10^{-5}$—6.6×10^{-6}cm^2/s thereafter. Data in Figure 4 confirm the known MCT tendency to predict a glass transition at state points where the dynamics of the real system is still ergodic.

The main results of this work are presented in Figure 5, where the glass transition line identified through MCT calculations is displayed. We also report in the same figure the theoretical predictions from MHNC calculations at $T = 1200$ and 3500 K, our previous MD data for vitrification,[2,3] and the estimate of ref 19. MHNC calculations follow the general approach already employed successfully to predict the liquid−vapor coexistence of the C_{60} model at issue.[23] The numerical solutions of the MCT long-time limit equations (the non-ergodicity factors) across the vitrification thresholds are shown in Figure 6, for several isobaric paths investigated in this work. The last ergodic state points ($f_k = 0$) and the first nonergodic ones ($f_k \neq 0$) are assumed to bracket the ideal MCT glass transition line reported in Figure 5. The distances in the $\rho-T$ plane among these couple of points hence constitute the error bars of our predictions.

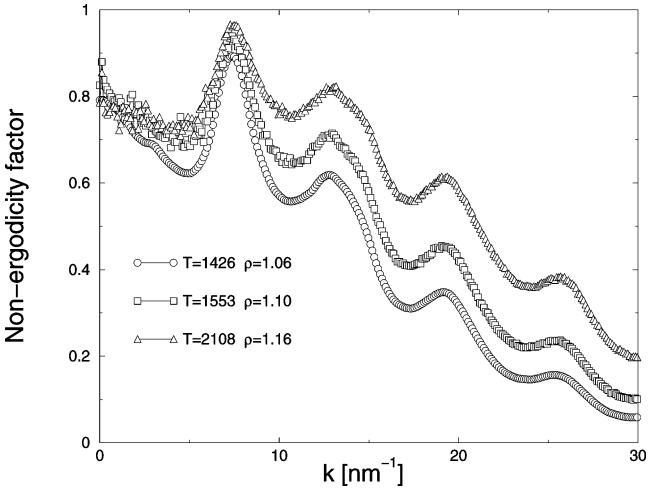

Figure 6. Nonzero ergodicity factors at the MCT transition thresholds (f_k^c) for pressures $P = 250$, 40, and 3.5 MPa (from top to bottom). State points along such isobaric paths with temperatures immediately higher than those reported in the figure are still ergodic, i.e., $f_k = 0$. Densities and temperatures in the legends are expressed in nm^{-3} and K, respectively.

It appears from Figure 5 that the MCT glass transition line does not show re-entrant behavior and is reasonably parallel to the vitrification locus obtained in our previous MD simulation study[2,3] (we shall further comment about these specific features of our results), and runs fairly close to the one determined through MCT and HNC or PY structure factors as input data in ref 19. In particular, PY predictions tend to slightly underestimate the vitrification density, and the HNC results are generally more accurate over the temperature regime investigated.

Our test MHNC and HNC calculations, limited to some selected densities along the isotherms $T = 3500$ and 1200 K are also reported in Figure 5 and confirm the trend illustrated above. A comparison between theoretical and simulation structure factors is reported in Figure 7. We display in particular data at the highest temperature and density investigated in this work, namely $T = 3500$ K and $\rho = 1.15$ nm^{-3}, and data at the opposite extremum, i.e., $T = 1200$ K and $\rho = 1.05$ nm^{-3} (the lowest state point which we have been able to investigate before the system displays a pronounced tendency to phase separate). Apart from the well-known difficulties of the theoretical tools employed to closely follow the $k \rightarrow 0$ behavior of the structure factor, especially in the proximity of the phase separation, it appears that both theories slightly underestimate the height of the main peak (with MHNC theory performing better than HNC), and a small dephasing emerges in the position of the secondary peaks at higher k vectors. On the whole, we judge the agreement between theory and simulations quite satisfactory, especially if we take into account that all data recorded in Figure 7 have been obtained by pushing the integral equation scheme toward "extreme conditions", as far as the regime in which such tools are known to give the best performances is concerned.

Figures 5 and 7 document the good agreement between present simulation results, our thoretical predictions, and those obtained by Greenall and Voigtmann,[19] equally from the point of view of the MCT transition threshold and at the level of input structure factor calculations. Our evidence indirectly support the conclusions drawn in ref 19 that, in the framework provided

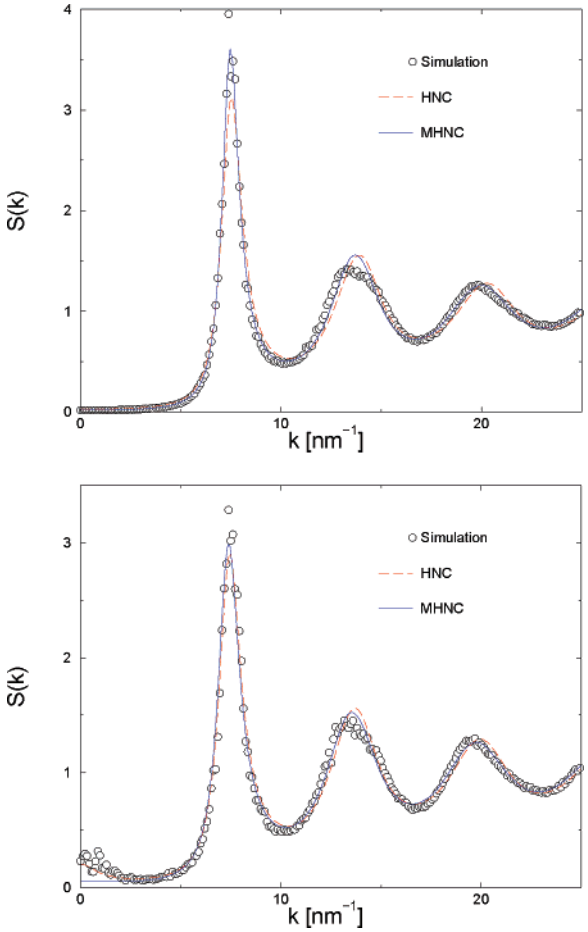

Figure 7. Comparison between theoretical and simulation results for the static structure factors at $T = 3500$ K and $\rho = 1.15$ nm^{-3} (top) and $T = 1200$ K and $\rho = 1.050$ nm^{-3} (bottom).

by the mode-coupling theory, and in the thermodynamic region $T \lesssim 3000$ K, the attractive part of the Girifalco potential is short-range enough to begin to influence the approach to the structural arrest of the system. The arguments presented in ref 19 are based in particular to an extended analysis of the properties of the nonergodicity factor, together with a comparison between the MCT lines obtained with either the full C_{60} potential or with a truncated version, where the attractive part is cut off according to the WCA procedure.[26]

We now turn to the examination of the low-temperature regime MCT results. As visible in the top panel of Figure 2, at $T = 1200$ K, MCT predicts the existence of a glassy phase for $\rho = 1.05$ nm^{-3}, which corresponds, as discussed above, to the lowest density for which a genuine homogeneous sample is observed during the time of our MD simulations, whereas the tendency of the system to phase separate is already well under way at $\rho = 1.025$ nm^{-3}. For this reason, and in view of the fact that MCT itself strictly deals with homogeneous systems, we estimate the vitrification density at $T = 1200$ K as falling halfway between $\rho = 1.025$ and 1.05 nm^{-3}; this value, reported in Figure 5, nicely coincides with our MHNC estimates. If lower density, but phase-separated, MD structure factors are fed into the MCT equations, glass states are equally predicted. The reason for such an outcome can be appreciated if we observe, again in Figure 2, the way the differences in the shape of the various structure factors reflect in the corresponding nonergodicity factors: it appears that, in passing from $\rho = 1.050$ to 0.950 nm^{-3}, the structure factor displays minor differences (especially in the sensitive region of the nearest-neighbor peak) except for the already commented steep rise at $k = 0$. By contrast, the nonergodicity factors, also shown in the same figure, are hardly affected by the density variation and infact run almost superimposed on top of each other, thus predicting a glassy phase all along the isotherm $T = 1200$ K. Our results are consistant with the theoretical observation that MCT predictions for glasses characterized by short-range attractions, are barely sensitive to the low-k behavior of the structure factor.[21]

TABLE 1: Comparison, for Several Temperatures, among the MCT Transition Densities Calculated in this Work (Column 2), the MD Results of Refs 2 and 3 (Column 3) and the Estimates which Are Obtained if We Apply a 12% Shift to MCT Data (Column 4)[a]

T	MCT	MD	MCT (shifted)
1635	1.073	1.190	1.206
1478	1.050	1.187	1.180
1200	1.037	1.177	1.166

[a] Temperatures are given in K, and densities are in nm^{-3}.

The nonzero ergodicity factors displayed in Figure 2 would allow us to shift to lower densities the $T = 1200$ K MCT vitrification threshold, causing a net bending of the glass transition line, even more pronounced than that predicted in ref 19. Although this feature would indicate an enhancement of the attraction-driven properties of the glass phase, the tendency to phase separate of our sample detected during MD simulations prompts us to some caution as far as any definite conclusion about this point is concerned. Similar problems with the phase separation of the sample prevented us from investigating the vitrification threshold for temperatures $T < 1200$ K. More extensive simulations, accompanied by an analysis of the size dependence of the results, might be worth it, in this respect. Such a program however is unlikely to be implemented easily, given the fact that the thermodynamic region to be explored falls well beneath the metastable liquid−vapor binodal line of C_{60}, and definitely inside the solid−vapor metastable equilibrium region, both circumstances implying a strong trend to phase separation.

In comparison with our previous MD estimates of the glass transition of the Girifalco C_{60} model,[2,3] based on several structural and dynamic indicators, the MCT predictions moderately underestimate the transition densities. It is well-known that a corresponding underestimate occurs when reference MCT predictions for hard spheres ($\eta_{glass} = \pi/6\rho\sigma^3 = 0.516$[27]) are compared with the rigorous computer simulation result ($\eta_{glass} = 0.58$[28]). In this case, a common procedure has been to exploit such a ∼12% discrepancy, in order to sistematically shift to higher densities the MCT vitrification curves, also for other models, when a comparison with simulation data is carried out (see, e.g., ref 14). If we apply the same correction to our MCT points, we obtain the remarkable agreement with MD estimates reported in Table 1. In refs 2 and 3, we have shown that all vitrification densities reported in Figure 5 nicely fall on a single value ($(\pi/6\rho\sigma_{eff}^3 \simeq 0.58$, almost coincident with the hard-sphere glass transition density), on condition that all data are rescaled through the effective (temperature dependent) diameter σ_{eff} which is obtained by substituting the soft repulsive part of the Girifalco potential with a pure hard-core exclusion, according to the WCA prescription.[26] As a consequence, we have deduced in refs 2 and 3 that the hard-sphere behavior plays the main role in determining the structure of the C_{60} glass, which hence results essentially repulsion-driven in nature. In order to reconcile the attractive nature of the MCT glass discussed in ref 19 with the results of refs 2 and 3, it is worth observing in Figure 5 that in the low temperatures regime the bending of

the MD curve is milder, with respect to the MCT predictions. In this case, it could be possible that, on lowering the temperature further, also the glass observed in our previous studies would display more pronounced attraction-driven effects. On the other hand, the analysis carried out in this work indicates that the strong tendency of the system to phase separate would likely preclude the possibility of extracting a meaningful and robust conclusion from an investigation of the behavior of the C_{60} model in this (highly metastable) low-temperature, high-density regime.

4. Conclusions

We have reported an MCT determination of the glass transition line in a model C_{60}. The theoretical calculations are based on the use, as input data for the MCT equations, of structure factors obtained via an extensive molecular dynamics simulation investigation of the fullerene systems at various pressures. The shape of the vitrification locus is in fairly good agreement with our previous determinations of the glass transition entirely based on MD simulations.[2,3] In fact, the MCT predictions appear to overall underestimate the glass density by ~10% with respect to refs 2 and 3, manifesting an otherwise well-known inaccuracy of the theory. The present results are also in fairly good agreement with the glass transition line obtained by other authors through MCT calculations based on HNC structure factors input.[19] MCT calculations based on the refined modified HNC theoretical $S(k)$ are also presented in this work and reproduce faithfully the glass transition line.

As far as the interplay between the nonergodicity factors and the structure factors $S(k)$ is concerned, our evidence lends support to the theoretical analysis of ref 19, where the influence of the attractive part of the C_{60} potential on the structural arrest properties of the model is argued. Our simulations document a strong tendency of the system to phase separate in the low-temperature region where the MCT glass transition line should exhibit a more pronounced attraction-driven character. In this case, as required by MCT, we have restricted our analysis only to those temperatures and densities for which a fully homogeneous sample is obtained, this choice resulting in a glass line with a rather moderate bending. A more extensive computer simulation investigation, which takes into account for instance size effects, might be in order to further enlighten this point.

The picture emerging from the overall shape and characters of the glass transition line vs the repulsive-attractive potential features turns out to be consistent with the more general proposition that the glass line terminates on the liquid side of the liquid−gas coexistence, when particles interact with spherical potentials in which the excluded volume repulsion is complemented by attraction.[29,30] This scenario actually appears to be validated independently from the range of the attractive potential.[29] Nonspherical patchy potentials, in which the number of interacting particles is significantly reduced as compared to the spherical case, are necessary in order to suppress and shift to small densities the liquid−gas phase separation curve[31,32] and hence to extend the dynamic arrest line to lower temperatures and smaller densities.

Acknowledgment. This work has been done in the framework of the Marie Curie Network on Dynamical Arrest of Soft Matter and Colloids, Contract Nr MRTN-CT-2003-504712. D.C. acknowledges the financial support of the PI2S2 Project managed by the Consorzio COMETA, a project co-funded by the Italian Ministry of University and Research (MIUR) within the Piano Operativo Nazionale Ricerca Scientifica, Sviluppo Tecnologico, Alta Formazione (PON 2000-2006). More information is available at http://www.pi2s2.it and http://www.consorzio-cometa.it.

References and Notes

(1) Girifalco, L. F. *J. Phys. Chem.* **1992**, *96*, 858.
(2) Abramo, M. C.; Caccamo, C.; Costa, D; Ruberto, R. *J. Phys. Chem. B* **2004**, *108*, 13576.
(3) Abramo, M. C.; Caccamo, C.; Costa, D; Ruberto, R. *J. Phys. Chem. B* **2005**, *109*, 24077.
(4) Hagen, M. H. J.; Meijer, E. J.; Mooij, G. C. A. M.; Frenkel, D.; Lekkerkerker, H. N. W. *Nature* **1993**, *365*, 425.
(5) Cheng, A.; Klein, M. L.; Caccamo, C. *Phys. Rev. Lett.* **1993**, *71*, 1200.
(6) Costa, D.; Pellicane, G.; Abramo, M. C.; Caccamo, C. *J. Chem. Phys.* **2003**, *118*, 304.
(7) Hasegawa, M.; Ohno, K. *J. Chem. Phys.* **1999**, *111*, 5955.
(8) Muschol, M.; Rosenberger, F. *J. Chem. Phys.* **1997**, *107*, 1953.
(9) Rosenbaum, D. F.; Kulkarni, A.; Ramakrishnan, S.; Zukoski, C. F. *J. Chem. Phys.* **1999**, *111*, 9882.
(10) Piazza, R. *Curr. Opin. Colloid Interface Sci.* **2000**, *5*, 38.
(11) Poon, W. C. K. *Curr. Opin. Colloid Interface Sci.* **1998**, *3*, 953.
(12) Fabbian, L.; Götze, W.; Sciortino, F.; Tartaglia, P.; Thiery, F. *Phys. Rev. E* **1999**, *59*, R1347.
(13) Dawson, K. A. *Curr. Opin. Colloid Interface Sci.* **2002**, *7*, 218.
(14) Foffi, G.; McGullagh, G. D.; Lawlor, A.; Zaccarelli, E.; Dawson, K. A.; Sciortino, F.; Tartaglia, P.; Pini, D.; Stell, G. *Phys. Rev. E* **2002**, *65*, 031407.
(15) Sciortino, F.; Tartaglia, P. *Adv. Phys.* **2005**, *54*, 471.
(16) Götze, W. In *Liquids, freezing and the glass transition*; Hansen, J.-P., Levesque, D., Zinn-Justin, J., Eds.; North-Holland: Amsterdam, 1991.
(17) Dawson, K. A.; Foffi, G.; Fuchs, M.; Götze, W.; Sciortino, F.; Sperl, M.; Tartaglia, P.; Voigtmann, Th.; Zaccarelli, E. *Phys. Rev E* **2001**, *63*, 011401.
(18) Zaccarelli, E.; Foffi, G.; Tartaglia, P.; Sciortino F.; Dawson, A. K. *Phys. Rev. E* **2001**, *63*, 031501.
(19) Greenall, M. J.; Voigtmann, Th. *J. Chem. Phys.* **2006**, *125*, 194511.
(20) Hansen J.-P.; McDonald I. R. *Theory of Simple Liquids*, 2nd ed.; Academic Press: London, 1986.
(21) Greenall, M. J.; Voigtmann, Th.; Monthoux, P.; Cates, M. E. *Phys. Rev. E* **2006**, *73*, 050501.
(22) Rosenfeld, Y.; Ashcroft, N. W. *Phys. Rev. A* **1979**, *20*, 1208.
(23) Caccamo, C. *Phys. Rev. B* **1995**, *51*, 3387.
(24) Andersen, H. C. *J. Chem. Phys.* **1980**, *72*, 2384.
(25) Costa, D.; Pellicane, G.; Caccamo, C.; Schöll-Paschinger, E.; Kahl, G. *Phys. Rev. E* **2003**, *68*, 021104.
(26) Weeks, J. D.; Chandler, D.; Andersen, H. C. *J. Chem. Phys.* **1971**, *54*, 5237.
(27) Franosch, T.; Fuchs, M.; Götze, W.; Mayr, M. R.; Singh, A. P. *Phys. Rev. E* **1997**, *55*, 7153.
(28) Woodcock, L. V. *Ann. N.Y. Acad. Sci.* **1981**, *37*, 274.
(29) Foffi, G.; De Michele, C.; Sciortino, F.; Tartaglia, P. *Phys. Rev. Lett.* **2004**, *94*, 078301.
(30) Sastry, S. *Phys. Rev. Lett.* **2000**, *85*, 590.
(31) Zaccarelli, E.; Buldyrev, S. V.; La Nave, E.; Moreno, A. J.; Saika-Voivod, I.; Sciortino, F.; Tartaglia, P. *Phys. Rev. Lett.* **2005**, *94*, 218301.
(32) Bianchi, E.; Largo, J.; Tartaglia, P.; Zaccarelli, E.; Sciortino, F. *Phys. Rev. Lett.* **2006**, *97*, 168301.